pH sensing by FAK-His58 regulates focal adhesion remodeling

Chang-Hoon Choi,[1] Bradley A. Webb,[1] Michael S. Chimenti,[2] Matthew P. Jacobson,[2] and Diane L. Barber[1]

[1]Department of Cell and Tissue Biology and [2]Department of Pharmaceutical Chemistry, University of California, San Francisco, San Francisco, CA 94143

Intracellular pH (pHi) dynamics regulates diverse cellular processes, including remodeling of focal adhesions. We now report that focal adhesion kinase (FAK), a key regulator of focal adhesion remodeling, is a pH sensor responding to physiological changes in pH. The initial step in FAK activation is autophosphorylation of Tyr397, which increased with higher pHi. We used a genetically encoded biosensor to show increased pH at focal adhesions as they mature during cell spreading. We also show that cells with reduced pHi had attenuated FAK-pY397 as well as defective cell spreading and focal adhesions. Mutagenesis studies indicated FAK-His58 is critical for pH sensing and molecular dynamics simulations suggested a model in which His58 deprotonation drives conformational changes that may modulate accessibility of Tyr397 for autophosphorylation. Expression of FAK-H58A in fibroblasts was sufficient to restore defective autophosphorylation and cell spreading at low pHi. These data are relevant to understanding cancer metastasis, which is dependent on increased pHi and FAK activity.

Introduction

Remodeling of focal adhesions at cell–substrate attachment sites is necessary for tissue morphogenesis and cell migration. A key regulator of focal adhesion remodeling is the nonreceptor kinase focal adhesion kinase (FAK), which binds to the cytoplasmic domain of integrin β subunits and transduces integrin and growth factor signals for cell adhesion dynamics, migration, and survival (Almeida et al., 2000; Sieg et al., 2000; Webb et al., 2004). FAK is essential for embryonic development (Ilić et al., 1995), including neuronal pathfinding and epithelial and vascular morphogenesis (Ilic et al., 2003; Nikolopoulos and Giancotti, 2005). Consistent with promoting cell migration and survival, FAK is necessary for carcinogenesis (McLean et al., 2004; Provenzano et al., 2008; Pylayeva et al., 2009) and tumor angiogenesis (Tavora et al., 2010). Hence, how FAK activity is regulated impacts our understanding of normal and pathological cell behaviors.

Activation of FAK requires first autophosphorylation of a noncatalytic Tyr397 and then phosphorylation of catalytic Tyr576 and Tyr577. Crystal structures of FAK reveal that these events are associated with conformational changes between autoinhibited and active states (Lietha et al., 2007). Autophosphorylated Tyr397 (pY397), located in a flexible linker between an N-terminal band 4.1, ezrin, radixin, moesin (FERM) domain and a central kinase domain, docks the SH2 domain of Src family kinases (Lim et al., 2008). Docked Src kinases phosphorylate FAK-Tyr576 and Tyr577 in the activation loop to increase FAK catalytic activity. The autoinhibited conformation includes multiple interactions between FERM and kinase domains that sterically block the active site cleft. Additionally, the F1 lobe of the FERM domain sequesters the flexible linker, making Tyr397 inaccessible for phosphorylation. Although structural data indicate that displacement of the FERM domain from the kinase domain is necessary for autophosphorylation (Lietha et al., 2007), how this is initiated remains incompletely understood. Suggested naturally occurring in trans mechanisms include docking of an unspecified activating protein (Lietha et al., 2007), binding to the cytoplasmic domain of integrin β subunits (Schaller et al., 1995; Cooper et al., 2003), and transphosphorylation by FAK clustering (Arold, 2011). We now show that FAK is directly sensitive to physiological changes in pH and an alkaline pH induces conformational changes that allow autophosphorylation of Tyr397. Our findings are relevant for cancer cell biology because most carcinomas have an alkaline intracellular pH (pHi; Webb et al., 2011).

THE JOURNAL OF CELL BIOLOGY

Results and discussion

We previously reported that fibroblasts deficient for the plasma membrane Na-H exchanger NHE1 that mediates efflux of intracellular H^+ have decreased pHi and impaired cell migration with prolonged focal adhesion turnover (Denker and Barber, 2002; Srivastava et al., 2008). We also showed that decreased pHi attenuates FAK-pY397 with integrin activation (Tominaga and Barber, 1998; Karydis et al., 2009). FAK promotes focal adhesion remodeling not by regulating the assembly of new focal contacts, but by being necessary for the efficient disassembly of nascent adhesions (Ilić et al., 1995; Webb et al., 2004). How FAK activity promotes focal adhesion turnover is incompletely understood but requires pY397 because impaired turnover in FAK-null mouse embryonic fibroblasts (MEFs) is restored by expression of wild-type FAK but not FAK-Y397F (Webb et al., 2004). To test whether increased pHi is necessary for increased FAK-pY397 during cell spreading, we lowered pHi in MEFs by suppressing NHE1 expression using lentivirus-mediated shRNA infection. We confirmed decreased NHE1 expression by immunoblotting (Fig. 1 A) and loss of activity by measuring the rate of pHi recovery from an acid load (Fig. S1, A and B). The steady-state pHi of 7.26 ± 0.05 with NHE1 shRNA was lower than the pHi of 7.48 ± 0.06 and 7.45 ± 0.04 in wild-type and nontargeting (NT) shRNA cells, respectively. NHE1 shRNA cells had significantly decreased FAK-pY397 and pY576/7 after plating on fibronectin compared with controls (Fig. 1, B and C). In contrast, NHE1 shRNA had no effect on autophosphorylation of Src-Tyr416, which increases with cell attachment but independently of FAK (Fig. S1 C; Arias-Salgado et al., 2003).

Consistent with decreased FAK-pY397 and pY576/7, MEFs expressing NHE1 shRNA had defective cell spreading on fibronectin compared with wild-type and NT cells (Fig. 1 D). Cells fixed at the indicated times after plating were immunolabeled with antibodies to the focal adhesion–associated proteins paxillin (Fig. 1 D) and vinculin (Fig. S1 D). NHE1 shRNA cells formed nascent focal adhesions at 20 min but were less spread at 60 min, as indicated by a more round morphology, and had significantly smaller (Fig. 1 E) and more (Fig. S1 E) focal adhesions compared with controls. Additionally, HaCaT keratinocytes pretreated for 30 min with the NHE1 inhibitor 5 (N-ethyl-N-isopropyl)amiloride (EIPA), which we confirmed decreases NHE1 activity (Fig. S1 F), had attenuated FAK-pY397 (Fig. S1 G) and limited spreading (Fig. S1 H) on fibronectin compared with control HaCaT cells. EIPA also attenuated FAK-pY397 in MDA-MB-231 human mammary adenocarcinoma cells (Fig. S1 I). NHE1-dependent defects in cell spreading are similar to FAK-null MEFs (Owen et al., 1999; Sieg et al., 1999) (see Fig. 5 D), suggesting a critical role for NHE1 activity in early cell spreading on fibronectin. Additionally, these data are consistent with loss of NHE1 activity attenuating cell attachment (Tominaga and Barber, 1998) and the mechanostability of focal adhesions being pH dependent (Beaumont and Mrksich, 2012). We also found that pHi regulated FAK-pY397 in NHE1-deficient PS120 cells, which have attenuated FAK-pY397 compared with parental CCL39 fibroblasts (Fig. S1 J; Tominaga and Barber, 1998; Karydis et al., 2009). With plating on fibronectin, lowering pHi

by an NH_4Cl-induced acid load decreased FAK-pY397 and raising pHi by incubating cells at 15% CO_2 in medium containing 50 mM HCO_3^- increased FAK-pY397 compared with controls maintained at 5% CO_2 with 25 mM HCO_3^-. However, changing pHi was not sufficient to regulate FAK-pY397 in cells plated on poly-L-lysine (Fig. S1 J), suggesting that integrin activation is necessary.

Activation of integrin receptors increases NHE1 activity and pHi (Schwartz et al., 1991; Demaurex et al., 1996; Tominaga and Barber, 1998). Whether there are pH changes at focal adhesions during cell spreading, however, has not been reported. To answer this question, we used TIRF microscopy to image pH dynamics in spreading MEFs expressing paxillin fused to the pH biosensor pHluorin and to mCherry. The fluorescence of pHluorin, a pH-sensitive variant of GFP, increases at higher pH but the fluorescence of mCherry is pH insensitive and indicates abundance of the probe (Koivusalo et al., 2010). Fluorescence ratios were converted to pH values by terminating each experiment with a nigericin buffer at specific pH values, which confirmed pH-dependent changes in pHluorin intensity (Fig. S2 A). Wild-type MEFs expressing paxillin-mCherry-pHluorin had focal adhesions with normal morphology and dynamics (Fig. 1 F), suggesting that the probe did not interfere with these parameters. In control cells the fluorescence ratio increased as focal adhesions matured during cell spreading (Fig. 1 F), being significantly greater at 50 min than at 30 min (Fig. 1, F and G). In NHE1 shRNA cells the mCherry signal showed that focal adhesions remained small over time (Fig. S2 B), which is consistent with paxillin and vinculin immunolabeling (Fig. 1 D; Fig. S1 D). In NHE1 shRNA cells the fluorescence ratio did not increase at focal adhesions, but we were unable to determine pH values, as the focal adhesions were too small and unstable to calibrate the signal with nigericin (Fig. S2 B). However, cytoplasmic pH remained constant at 30 and 50 min after plating (Fig. S2 C). These data show an NHE1-dependent increase in pH at focal adhesions with plating on fibronectin and that preventing increased pHi by suppressing NHE1 expression impairs cell spreading and focal adhesion morphology. Whether NHE1 localizes at focal adhesions remains controversial. We find that although NHE1 is enriched at the distal margin of membrane protrusions, it does not colocalize with paxillin (Denker et al., 2000; Denker and Barber, 2002). In contrast, colocalization is suggested by immunolabeling studies (Grinstein et al., 1993) and a recent proteomic profile of focal adhesion complexes that includes NHE1 (Kuo et al., 2011).

We next asked whether FAK autophosphorylation is directly pH sensitive. Because integrin $\alpha_v\beta_3$ activity is regulated by extracellular pH (Paradise et al., 2011), increased extracellular pH from inhibiting NHE1-dependent H^+ efflux might impair integrin signaling. However, activating integrins with $MnCl_2$ did not rescue decreased FAK-pY397 in HaCaT cells treated with EIPA (Fig. S3). Using in vitro kinase assays with recombinant mouse FAK confirmed direct regulation of FAK-pY397 by pH. Recombinant FAK containing the FERM (F) and kinase (K) domains and the interdomain linker (L) had a time-dependent increase in FAK-pY397 at pH 7.5 and 7.2 that was markedly less at pH 6.8 and 6.5 (Fig. 2, A and C). Hence, a higher pH is
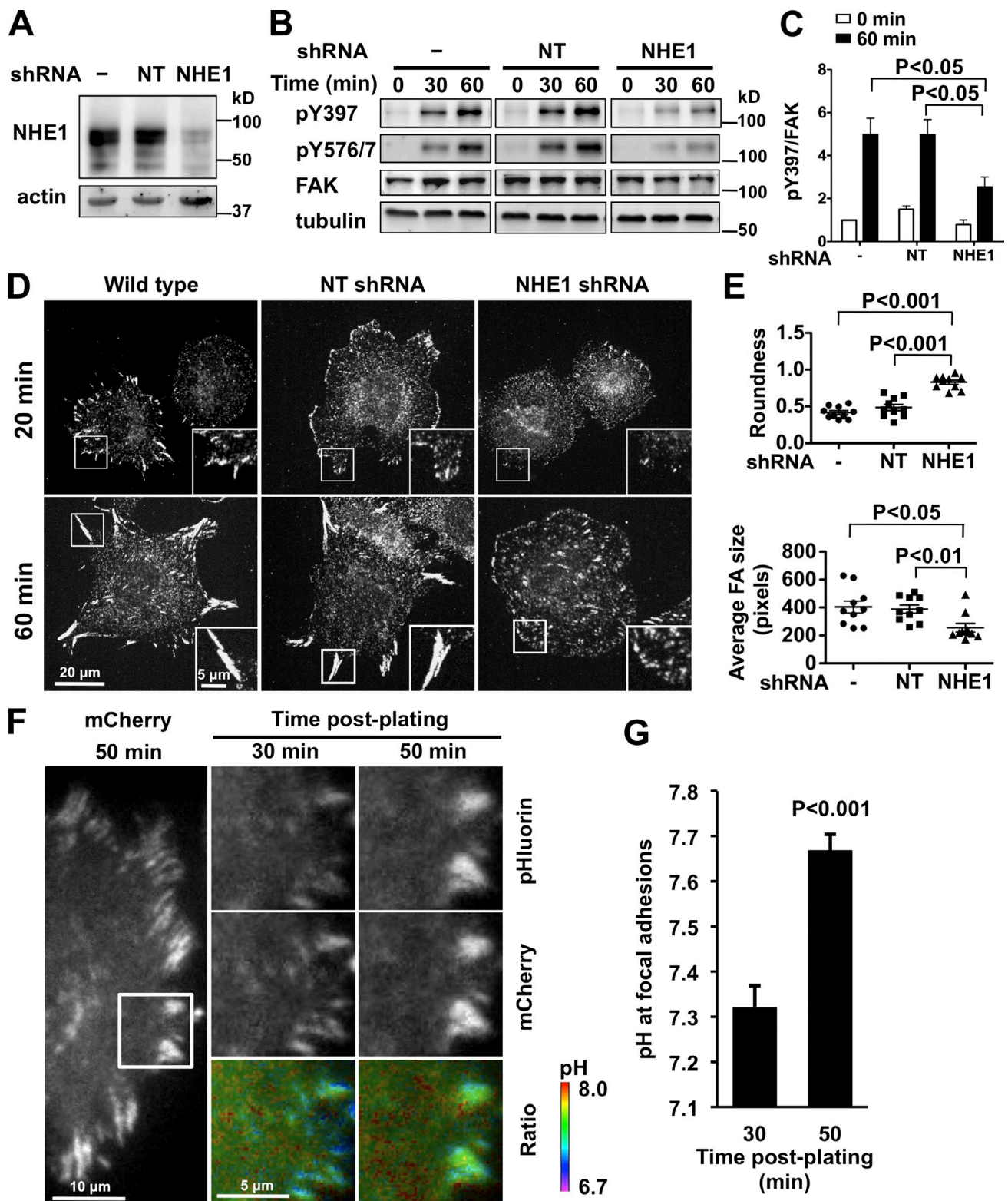
Figure 1.   **NHE1 shRNA and decreased pHi inhibit FAK-pY397 and cell spreading.** (A) Decreased NHE1 expression in MEFs infected with lentivirus encoding NHE1 shRNA compared with uninfected (−) cells and cells infected with nontargeting (NT) shRNA, determined by immunoblotting cell lysates. (B) FAK-pY397 and -pY576 were attenuated with NHE1 shRNA compared with control (−) and NT shRNA, as indicated by immunoblotting lysates of cells in suspension (0 min) and plated on fibronectin (60 min). (C) Abundance of FAK-pY397 relative to total FAK at the indicated times on fibronectin. Data are means ± SEM of three cell preparations. (D and E) In MEFs plated on fibronectin for 20 and 60 min and immunolabeled with anti-paxillin antibodies, NHE1 shRNA impairs cell spreading, indicated by roundness index, and focal adhesion size compared with control (−) and NT shRNA. Insets are enlarged images of boxed areas of representative focal adhesions. (F) Time-dependent increase in pH at focal adhesions with plating on fibronectin determined by TIRF ratiometric imaging of pH-sensitive pHluorin and pH-insensitive mCherry fused to paxillin. 10-µm × 10-µm images of cells (marked at left panel) at 30 and 50 min are shown. (G) Mean pH ± SEM of five focal adhesions at 30 and 50 min are representative of cells from three independent preparations.
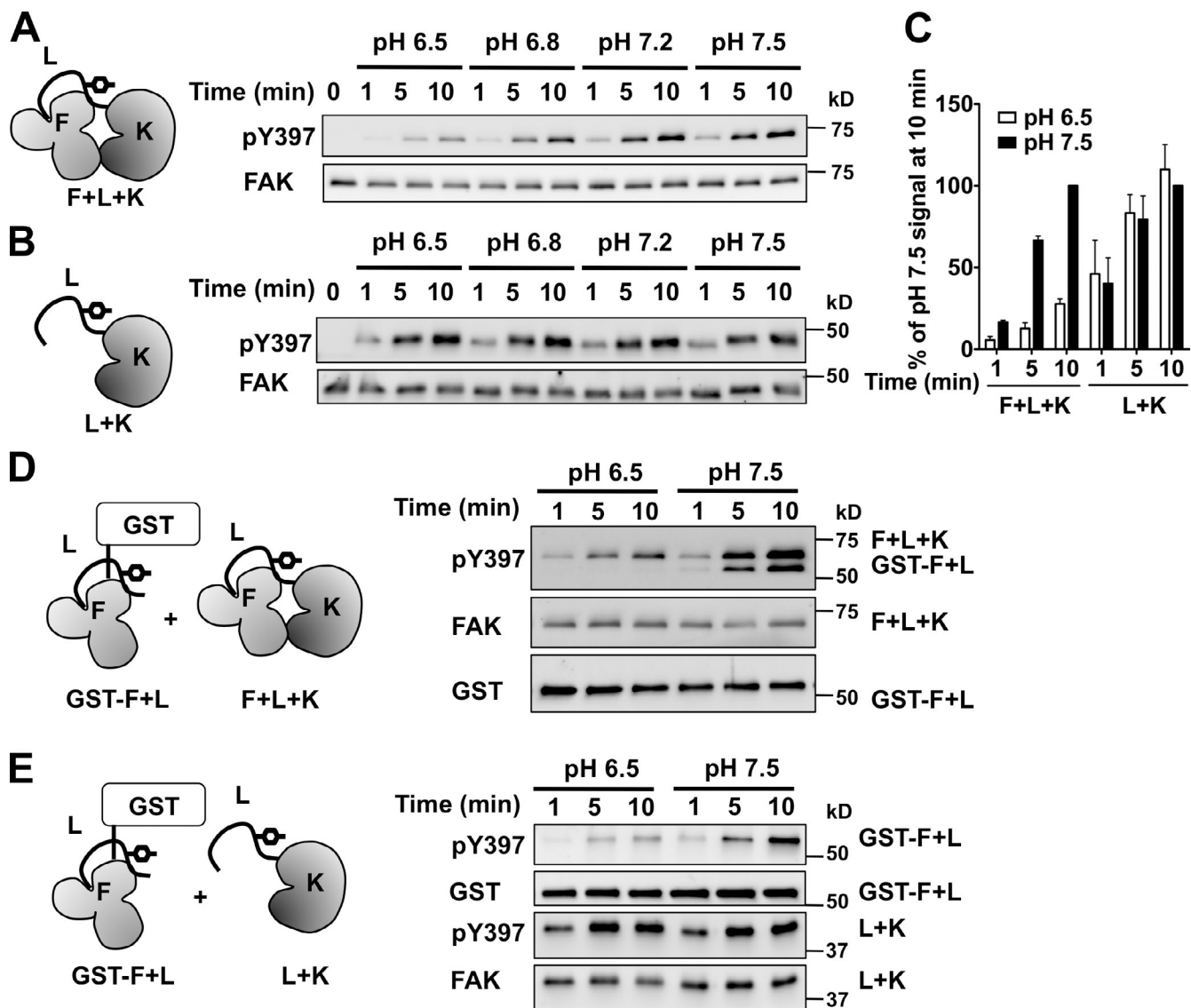
Figure 2. FAK autophosphorylation is pH dependent in vitro. (A) Time- and pH-dependent increase in pY397 of recombinant FAK containing the FERM domain (F), interdomain linker (L), and kinase domain (K). (B) Time-dependent increase in pY397 with L and K but lacking F is pH independent. (C) Abundance of pY397 relative to pH 7.5. Data are means ± SEM of the indicated constructs from A and B from three independent experiments. (D and E) Time- and pH-dependent increase in pY397 of a GST fusion of F and L induced in trans by F and L and K (D) or by L and K (E).

sufficient to increase FAK-pY397 in vitro, in contrast to integrin activation also being required in cells.

We found that the FERM domain is necessary for pH-dependent pY397. A construct containing the interdomain linker and the kinase domain but lacking the FERM domain had a time-dependent increase in pY397 that was similar at pH values we tested from 6.5 to 7.5 (Fig. 2, B and C). Further confirming the role of the FERM domain, a GST fusion of the FERM domain and the interdomain linker had pH-dependent pY397 in trans by incubating with either FERM and kinase (Fig. 2 D) or only the kinase domain (Fig. 2 E).

The crystal structure of autoinhibited FAK indicates that the F1 lobe of the FERM domain sequesters the interdomain linker containing Tyr397 to prevent autophosphorylation (Lietha et al., 2007). We identified seven histidine residues, an unusually high number, clustered in the F1 lobe of FERM domain that

are unique to FAK and not found in FERM domains of other proteins. His41 and His75 are at the interface between the F1 lobe and kinase C-lobe, and His58 is close to Tyr397 (Fig. 3 A). The other four histidines are clustered at the interface between the F1 and F3 lobes and are also present in the F1 lobe of the FAK-related kinase Pyk2 (PDB 4EKU) that lacks cognate histidine residues at the kinase interface and adjacent to the linker. With a pK_a near neutral, histidines can titrate within the range of physiological pHi changes (Srivastava et al., 2007; Schönichen et al., 2013). We reasoned that protonation of His41, His58, or His75 at lower pH might confer an electrostatic interaction maintaining an autoinhibited FAK conformation that is disrupted with neutral histidine residues at higher pH. To test this prediction we substituted these histidines with alanine to mimic a deprotonated residue and determined pY397 with a GST fusion of the FERM domain and interdomain linker in trans by
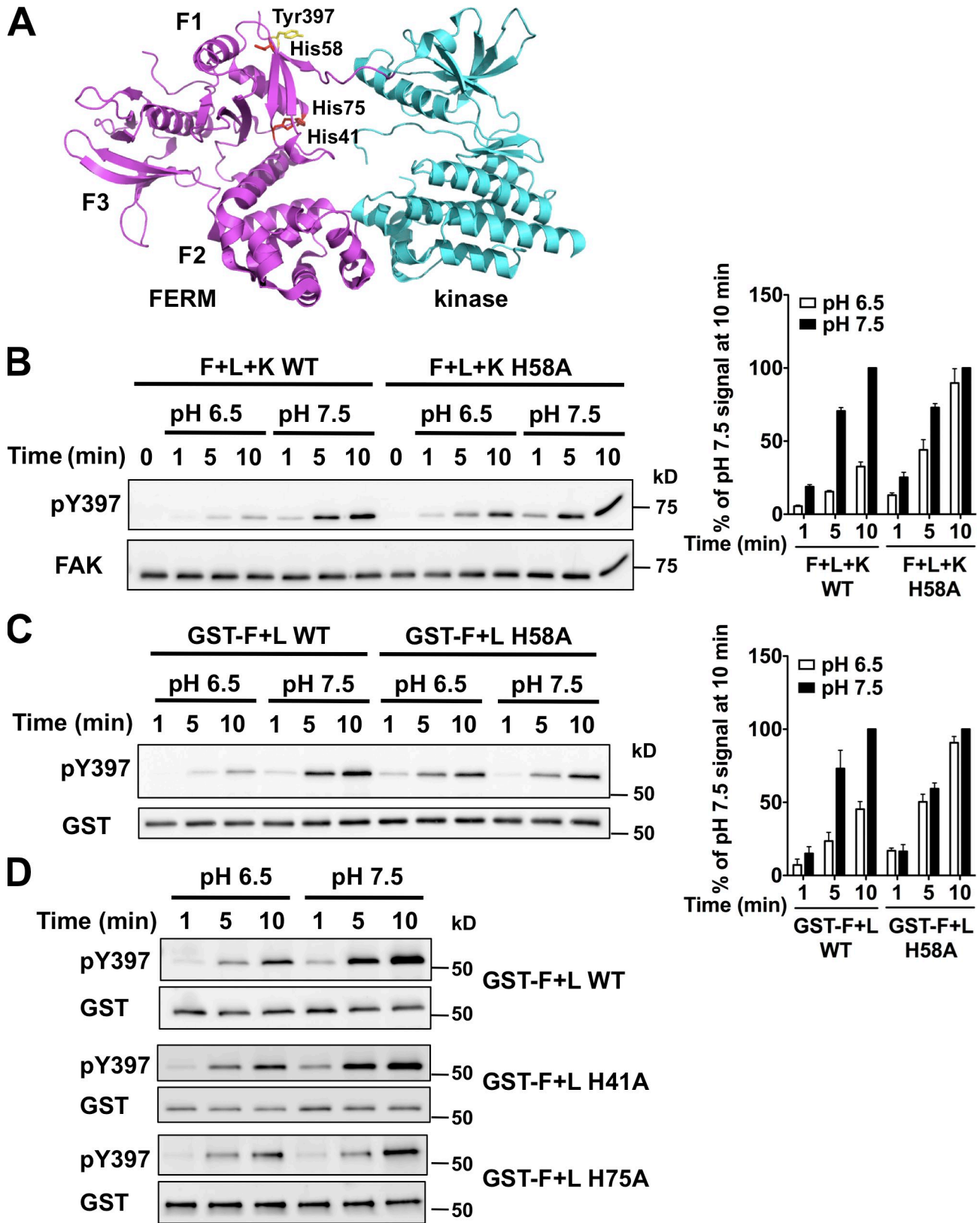
Figure 3. **His58 confers pH-dependent FAK-pY397.** (A) Structure of avian FAK (PDB 2J0J) showing His41 and His75 in the F1 lobe of the FERM domain at the interface with the kinase domain and His58 in close proximity to the interdomain linker. (B) Left immunoblot shows attenuated pY397 in wild-type FAK at pH 6.5 is restored in FAK-H58A. Right histogram shows abundance of pY397 relative to wild-type FAK at pH 7.5 (means ± SEM; n = 3). (C) Time-dependent increase in pY397 of FERM H58A in trans by the kinase domain is pH independent. (D) Time-dependent increase in pY397 of FERM H41A and H75A in trans by the kinase domain is pH dependent.
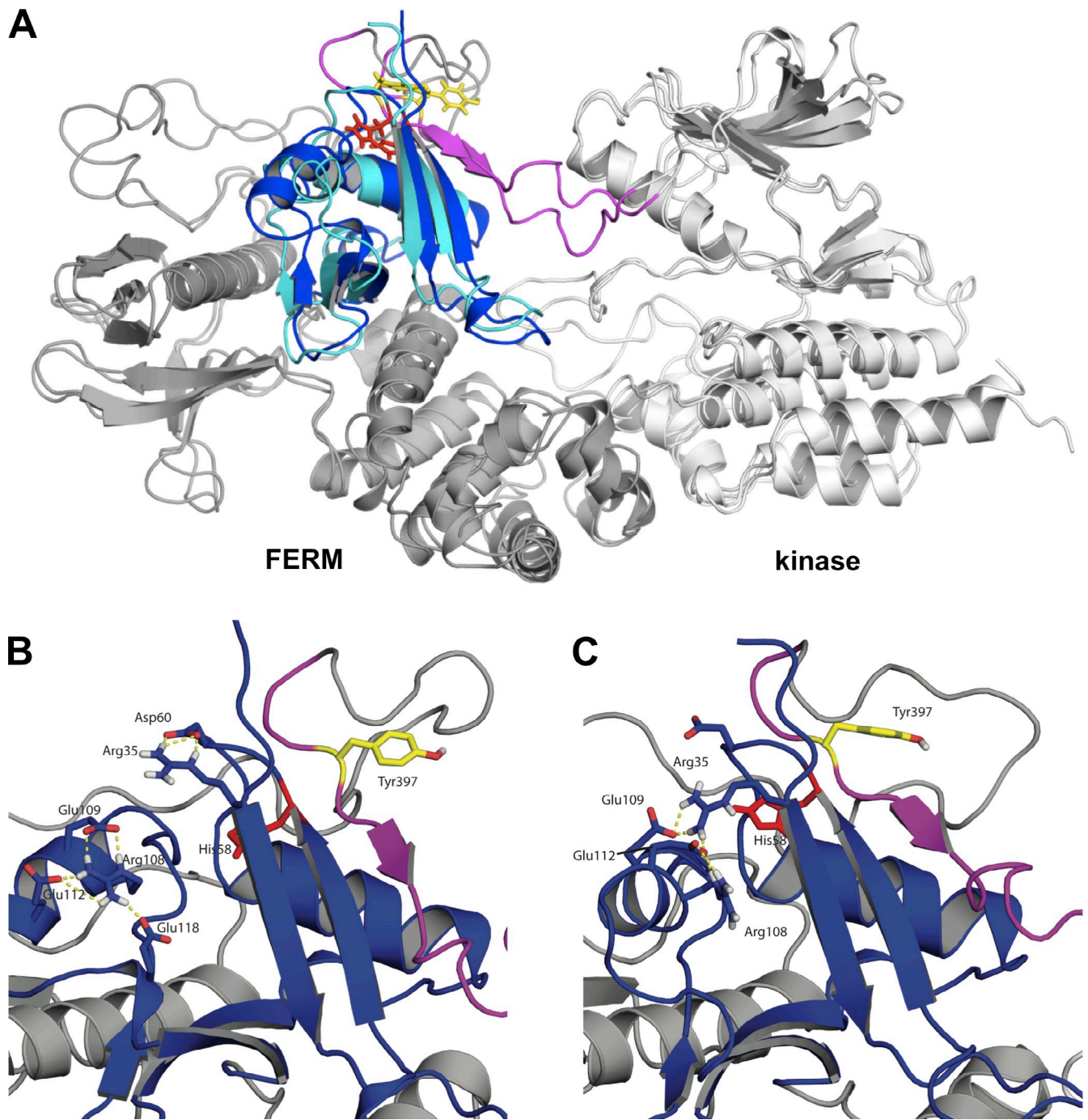
Figure 4. **Deprotonation of His58 facilitates conformational changes associated with autophosphorylation.** (A) Deprotonation of His58 facilitates conformational changes in the vicinity of the linker and Tyr397. Representative structures from simulations with His58 neutral (blue) and charged (cyan) are superimposed. For both representative structures, the side chain of Tyr397 is shown in yellow, His58 in red, and the linker region in magenta. (B and C) Close-up views of regions surrounding His58 and Tyr397 for neutral His58 (B) and positively charged His58 (C), highlighting changes in the network of electrostatic interactions of charged side chains.

FERM and kinase or the kinase domain. The H58A mutation had no effect on the abundance of pY397 at pH 7.5 compared with wild-type FAK, but conferred pH-independent pY397 that was similar at pH 6.5 and 7.5 (Fig. 3, B and C). In contrast, H41A and H75A mutations retained pH-sensitive pY397 that was similar to wild type (Fig. 3 D). These data suggest that His58 but not His41 or His75 confers pH-regulated autophosphorylation of FAK.

Molecular dynamics simulations were used to investigate how changes in the protonation state of His58 may promote conformational changes that facilitate autophosphorylation. We performed two 10-ns explicit solvent simulations, with His58 either neutral or positively charged, and all other His residues assigned to the neutral Nδ1 tautomer. Comparing the most highly populated conformers from each of the simulations revealed significant and persistent conformational changes (Fig. 4 A)

centered on the β-sheet containing the linker and Tyr397, as well as the orientation of the F1-α2 helix and the electrostatic network of Arg and Glu residues in the F1 domain. Although we did not observe complete detachment of the linker region during these short simulations, as might be expected to be necessary for Tyr397 phosphorylation, the environment of the Tyr397 side chain varied significantly between the simulations, despite the fact that it does not directly interact with His58. We speculate that the relatively large conformational changes associated with (de)protonation of His58 are due to the location of the side chain, which, although buried from solvent in the crystal structure, is located in the midst of a complex electrostatic network of charged side chains (Fig. 4, B and C). For His58 to facilitate conformational changes, its pK_a value in the autoinhibited state must be shifted with respect to that in the active state. The electrostatic interactions in this network may help maintain a more neutral-shifted pK_a value of His58. In this model, changing the protonation state of His58 rearranges the complex network of polar interactions, facilitating local conformational changes in the vicinity of the linker and Tyr397. The notion that electrostatic networks formed by ionizable groups in the F1 domain are critical for maintaining autoinhibition is also supported by mutational studies showing that loss of a Lys38 side-chain leads to hyperphosphorylation of Tyr397 (Cohen and Guan, 2005). We cannot conjecture, on the basis of these results, how these conformational changes might evolve over longer timescales or how they may ultimately facilitate autophosphorylation, but the model could be tested in future work by mutating other residues in the electrostatic network, which could also lead to pH-independent autophosphorylation.

FAK-pY397 and cell spreading were tested in MEFs transiently expressing FAK-His>Ala mutations tagged at the N terminus with GFP and the C terminus with an HA epitope. To resolve effects of heterologously expressed FAK independent of endogenous kinase we used FAK−/− MEFs. FAK-null mouse keratinocytes have increased NHE1 expression (Ilic et al., 2007), and although we found that FAK−/− MEFs have approximately twofold increased NHE1 abundance compared with FAK+/+ MEFs (unpublished data), their steady-state pHi of 7.46 ± 0.05 was not different than wild-type MEFs. FAK−/− MEFs plated on fibronectin for 60 min showed that compared with NT shRNA cells, NHE1 shRNA cells had attenuated pY397 with wild-type FAK and FAK-H75A but not with FAK-H58A (Fig. 5, A and B; P < 0.001), indicating rescue of autophosphorylation. Cell spreading of NHE1 shRNA cells was also restored with FAK-H58A. FAK−/− cells with NT shRNA had impaired cell spreading, as indicated by a rounded morphology, and smaller, more abundant focal complexes (Fig. 5, C and E) compared with FAK+/+ cells (Fig. 1 D). A similar phenotype was seen in FAK−/− cells expressing NHE1 shRNA (Fig. 5, D and E) and in noninfected controls (not depicted). Expression of wild-type FAK restored spreading and the size and abundance of focal adhesions in NT shRNA cells (Fig. 5 C) but not NHE1 shRNA cells (Fig. 5 D). In contrast, expression of FAK-H58A restored the spreading phenotype in both NT (Fig. 5, C and E) and NHE1 shRNA cells (Fig. 5, D and E). Rescue in NHE1 shRNA cells was not seen with FAK-H75A (Fig. 5, D and E) or with FAK-H41A (not

depicted). These data and our in vitro findings indicate that His58 confers pH-dependent FAK autophosphorylation.

Our results show pHi-dependent cell spreading and focal adhesion remodeling and reveal a molecular mechanism for pH-dependent FAK autophosphorylation. We previously reported that changes in pH allosterically regulate binding of the focal adhesion protein talin to actin filaments for efficient cell migration (Srivastava et al., 2008). Expression of a pH-insensitive talin partially rescues defects in focal adhesion remodeling and cell migration in the absence of NHE1 activity and low pHi. We predict a pH-independent FAK-H58A might also partially rescue these defects. However, because FAK-H58A mostly restored defective cell spreading at low pHi, pH-dependent talin–actin binding may be less important for cell spreading compared with focal adhesion remodeling during cell migration. These findings highlight how pHi dynamics regulates distinct proteins in unison to control complex cell behaviors, as suggested previously (Srivastava et al., 2007). Also possibly related to coordinated effects of pHi dynamics is that autophosphorylation of the FAK-related kinase Pyk2 increases at acidic pH (Li et al., 2004), although the molecular mechanism and functional significance of pH-dependent Pyk2 activity remains unknown. Moreover, our data support an increasingly evident role for protonation as a posttranslational modification regulating protein structure and function (Schönichen et al., 2013).

A pHi-dependent regulation of FAK activity is relevant to a number of human diseases. In some neurodegenerative disorders a constitutively decreased neuronal pHi limits neurite outgrowth and promotes cell death (Harguindey et al., 2007), which are also associated with decreased FAK activity (Huang et al., 2007; Chacón and Fazzari, 2011). Most cancer cells have a constitutively higher pHi than untransformed cells, which enables increased proliferation, survival, and metastatic progression (Cardone et al., 2005; Webb et al., 2011; Amith and Fliegel, 2013). These cell behaviors are also enabled by increased FAK activity (Almeida et al., 2000; Sieg et al., 2000; Webb et al., 2004). The ability of EIPA to attenuate FAK-pY397 in human adenocarcinoma cells (Fig. S1) together with previous findings on pHi regulating cell migration (Webb et al., 2011) suggest that preventing increased pHi could be a therapeutic strategy to limit cancer progression.

Materials and methods

Cell cultures and lentivirus
Mouse embryonic fibroblast (MEF) cells (provided by D.D. Schlaepfer, University of California, San Diego, La Jolla, CA) were plated on 0.1% gelatin-coated dishes and maintained in DMEM supplemented with 10% fetal bovine serum, nonessential amino acids, and sodium pyruvate at 5% CO_2. Human HaCaT keratinocytes and MDA-MB-231 human mammary adenocarcinoma cells were also cultured in the same medium. PS120 cells derived from the Chinese hamster lung CCL39 fibroblast line (Pouysségur et al., 1984) were cultured in DMEM supplemented with 5% fetal bovine serum. For silencing NHE1 expression, lentiviral shRNA constructs (TRCN0000044650 and TRCN0000313884) were purchased from Sigma-Aldrich. After 2 d of lentiviral infection, shRNA-expressing MEF cells were selected with 5 µg/ml puromycin. Knockdown of NHE1 was verified by immunoblotting with anti-NHE1 antibody (54; Santa Cruz Biotechnology, Inc.) and determining NHE1 activity as described previously (Denker et al., 2000). In brief, NHE1 activity was determined in a Hepes buffer (25 mM Hepes, 140 mM NaCl, 5 mM KCl, 10 mM glucose, 1 mM KPO_4, 1 mM $MgSO_4$, and 2 mM $CaCl_2$,
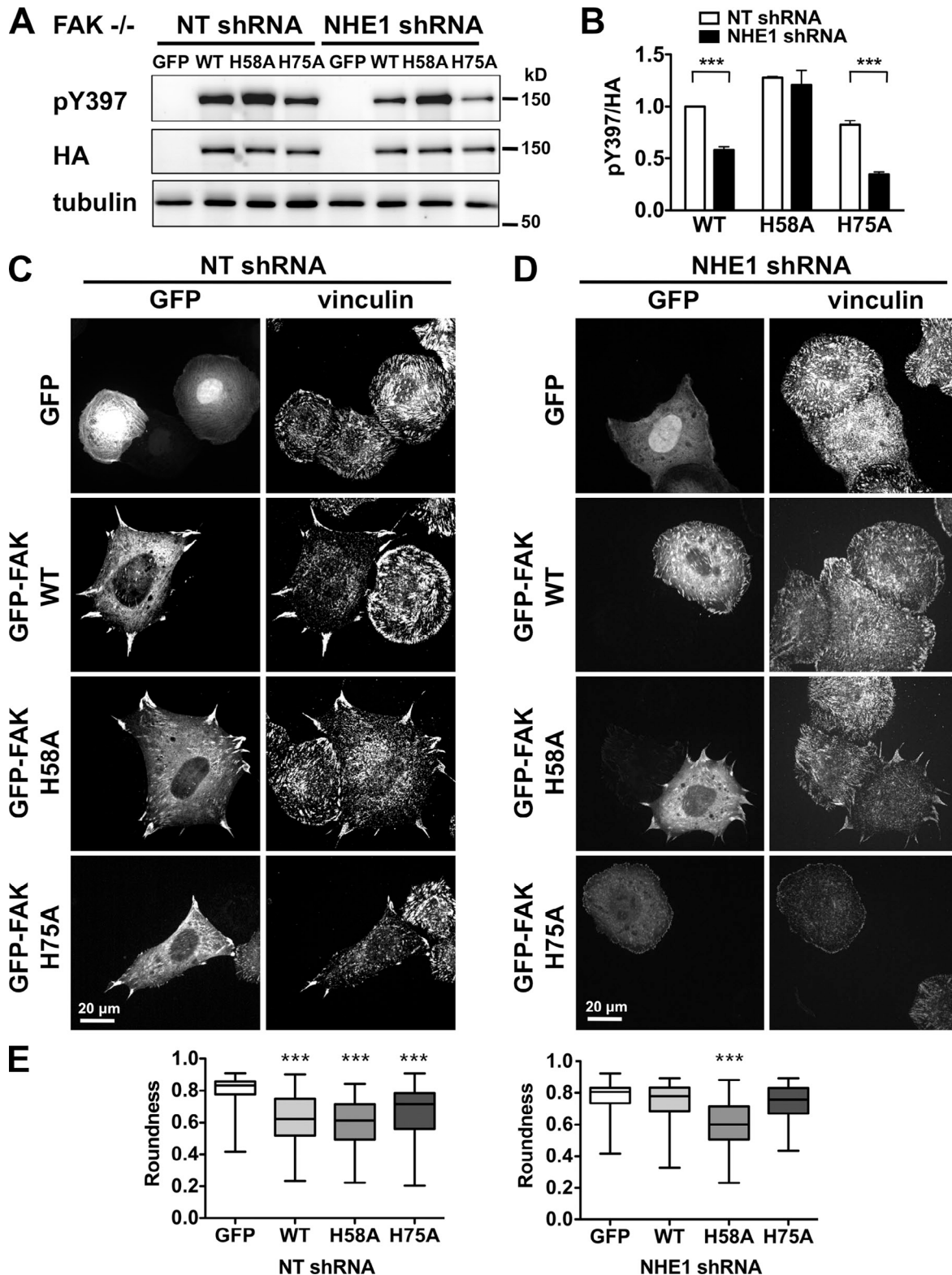
Figure 5. **FAK-H58A restores decreased pY397 and impaired cell spreading in FAK−/− MEF cells with NHE1 shRNA.** (A) Immunoblot indicates that abundance of pY397 with GFP-tagged FAK WT-HA and H75A-HA but not H58A-HA are markedly less with NHE1 shRNA compared with NT shRNA. Immunoblot with HA antibody shows expression of heterologously expressed FAK. (B) Abundance of pY397 relative to total FAK WT and mutants in cells from A. Data are means ± SEM of three cell preparations. Asterisks indicate significant difference of P < 0.001. (C) Impaired cell spreading and focal adhesion morphology in FAK−/− MEFs with NT shRNA, visualized by vinculin immunolabeling, are restored by expression of GFP-tagged FAK-WT, FAK-H58A, and FAK-H75A, but not GFP alone. (D) Impaired cell spreading and focal adhesion morphology in FAK−/− MEFs with NHE1 shRNA are restored by expression of FAK-H58A but not FAK-WT or FAK-H75A. (E) With NHE1 shRNA only H58A rescues spreading cell morphology scored by roundness. Data are from 75–100 cells analyzed in two cell preparations. Asterisks indicate significant difference of P < 0.001.

pH 7.4) by using cells loaded with 1 µM 2′,7′-bis-(2-carboxyethyl)-5-(and-6)-carboxyfluorescein (BCECF; Invitrogen) and measuring time-dependent pHi recovery from an NH$_4$Cl-induced acid load. Fluorescence of BCECF in an HCO$_3^-$ buffer (variation of Hepes buffer containing115 mM NaCl and Hepes replaced by 25 mM Na HCO$_3$) was used to determine steady-state pHi. The BCECF fluorescence at Ex490/Em530 and Ex440/Em530 was acquired every 15 s for 5 min using a plate reader (SpectraMax M5; Molecular Dynamics) and the fluorescence ratios were converted to pHi by calibrating each experiment with 10 µM nigericin in 105 mM KCl.

FAK constructs and transfection

Site-directed mutagenesis on GFP-FAK constructs (provided by D.D. Schlaepfer) was performed using the QuikChange Lightning kit (Agilent Technologies). Forward primers used for His-to-Ala substitutions were as follows: 5′-CGAG-TATTAAAGGTCTTTGCATATTTTGAAAGCAGTAGTGAG-3′ for H41A, 5′-CAGTATTATCAGGGCAGGAGATGCTACTGATG-3′ for H58A, and 5′-GAAGATAGTGGACAGTGCCAAAGTAAAGCACGTGG-3′ for H75A. The N-terminal fusion of paxillin to mCherry-pHluorin was generated by PCR amplifying the full length of paxillin cDNA for cloning into an Nhe1–XhoI site of mCherry-pHluorin plasmid (Koivusalo et al., 2010). GFP-FAK and paxillin-mCherry-pHluorin were transiently expressed in MEFs using jetPRIME (Polyplus) according to the manufacturer's instructions.

Cell plating, immunoblotting, and immunolabeling

Cells maintained in DMEM supplemented with 0.2% FBS for 16 h were trypsinized and resuspended in serum-free medium containing 0.5 mg/ml soybean trypsin inhibitor for 30 min and replated on coverslips or tissue culture plates coated with fibronectin (10 µg/ml) or poly-L-lysine as described previously (Karydis et al., 2009). At the indicated times, cells were fixed for immunolabeling or lysed for immunoblotting. To decrease pHi in the absence of NHE1, detached NHE1-deficient PS120 cells were resuspended in Hepes buffer containing 10 mM NH$_4$Cl for 20 min and washed with Hepes buffer without NH$_4$Cl before replating. To increase pHi in the absence of NHE1. PS120 cells were maintained for 24 h at 15% CO$_2$ in DMEM containing 50 mM HCO$_3^-$, detached as described above, resuspended in DMEM containing 50 mM HCO$_3^-$, and maintained at 15% CO$_2$ for 30 min before lysis. Total cell lysates for immunoblotting were prepared in RIPA lysis buffer (50 mM Hepes, pH 7.5, 150 mM NaCl, 1% Triton X-100, 1% sodium deoxycholate, 0.1% SDS, 10% glycerol, 1 mM MgCl$_2$, 1 mM EGTA, 1 mM sodium orthovanadate, 10 mM sodium pyrophosphate, 100 mM sodium fluoride, and protease inhibitor cocktail [Roche]). For immunoblotting, 5–10 µg of proteins were separated by SDS-PAGE and transferred to PVDF membrane (EMD Millipore). Membranes were blocked with 3% BSA for 30 min and probed with antibodies to FAK (1:1,000; BD), FAK-pY397 (1:1,000; EMD Millipore), FAK-pY576 (1:1,000; Cell Signaling Technology), Src (1:1,000; Santa Cruz Biotechnology, Inc.), Src-pY416 (1:1,000; Cell Signaling Technology), β-actin (1:2,500; EMD Millipore), and α-tubulin (1:2,500; Sigma-Aldrich). Bound antibody was detected by enhanced chemiluminescence (ECL; GE Healthcare).

For immunolabeling, cells were fixed with 4% formaldehyde for 12 min and permeabilized with 0.2% Triton X-100 for 10 min. After blocking for 1 h with 3% bovine serum albumin, cells were incubated with mouse paxillin antibodies (1:400; BD) or rabbit vinculin antibodies (1:400; Invitrogen) for 1 h followed by secondary goat anti–mouse antibodies conjugated with Alexa Fluor 488 (1:500; Invitrogen) or goat anti–rabbit antibodies conjugated with Alexa Fluor 568 (1:500, Invitrogen) for 1 h and then mounted in Mowiol (4-88; EMD Millipore). Images were acquired with a 60×/1.20 NA objective lens (Plan Apo; Nikon) on an inverted microscope (TE2000; Nikon) equipped with a spinning-disk unit (Yokogawa Corporation of America), 488-nm and 561-nm lasers, and a CoolSNAP HQ2 camera (Photometrics). Acquired images were managed by using NIS Elements software (Nikon) and focal adhesions were quantified by ImageJ (National Institutes of Health) using particle analysis function.

TIRF microscopy and ratiometric pH imaging

Live-cell TIRF microscopy was performed as described previously (Stehbens et al., 2012). In brief, images were acquired on a TI inverted microscope stand (Nikon) equipped with a motorized TIRF illuminator (Nikon), an iXon EMCCD camera (Andor Technology), and a 100×/1.49 NA objective (CFI APO TIRF; Nikon) using 1.5× intermediate magnification. All microscope hardware was controlled by NIS Elements software (Nikon) and an environmental chamber maintained the cells at 37°C and 5% CO$_2$. Supereclliptic pHluorin and mCherry signals were measured using 488-nm and 568-nm laser illumination, respectively. Before imaging, MEFs expressing paxillin-mCherry-SEpHluorin were plated onto 35-mm fibronectin-coated MatTek dishes and imaging began within 10 min of plating. Images were captured every 2 min for 1 h. At the end of the experiment, a nigericin clamp was performed to normalize pHi values by incubating cells for 5 min with 10 µM nigericin in 105 mM KCl at indicated pH values. Image manipulation and analysis was performed on Elements software (Nikon) and Microsoft Excel. All quantifications were performed on background-subtracted images. To measure the pH at focal adhesions of spread cells, ROIs were drawn around 14 focal adhesions per cell and the average pH of focal adhesion was calculated in each of 23 cells.

Recombinant protein expression and purification

Recombinant FAK FERM and kinase domains and FAK kinase domain were expressed using a baculovirus expression system (Invitrogen) according to the manufacturer's instructions. The cDNAs encoding mouse FAK FERM and kinase (amino aids 33–686) and kinase domain alone (amino acids 363–686) were amplified by PCR and subcloned into pFastBac HTb at the sites of BamHI and SalI. The recombinant bacmid DNAs were transfected into Sf21 cells using Cellfectin II (Invitrogen) and His-tagged FAK fragments were purified using Talon metal affinity resins (Takara Bio Inc.). To express FAK FERM domain (amino acids 1–400) in *Escherichia coli*, the cDNA was subcloned into pGEX6P-2 vector at the sites of BamHI and XhoI and the recombinant protein was expressed by the addition of 0.5 mM IPTG in *E. coli* BL21-DE3. GST-fused FAK/FERM fragments were purified using glutathione-agarose resins (Thermo Fisher Scientific).

In vitro kinase assays

For autophosphorylation assays, purified wild-type or mutant FAK FERM and kinase fragments were first dephosphorylated by incubation with the tyrosine-specific phosphatase YOP from *Yersinia entercolitica* for 30 min at 30°C and then treated with 2 mM sodium orthovanadate to inhibit YOP activity. The phosphorylation reaction was started by addition of an equal volume of 2× kinase buffer (100 mM Tris-HCl, 10 mM MgCl$_2$, 10 mM MnCl$_2$, and 5 mM ATP) and was stopped at the indicated times by addition of 5× SDS sample buffer. Aliquots of 30 ng of protein were separated by SDS-PAGE followed by immunoblotting with primary anti-pY397 or anti-FAK antibodies. After incubation with fluorescent secondary antibodies, the pY397 and FAK signals on the same blots were visualized using a Fluor-Chem Q (Alpha Innotech) with Cy5 and Cy3 filters, respectively. The relative amount of autophosphorylation was determined by the ratio of pY397 signals to FAK signals. For in-trans phosphorylation assay, GST-fused FERM protein (20 ng/µl) was pre-mixed in 2× kinase buffer and phosphorylation was started by mixing with dephosphorylated FAK kinase fragments. The relative amount of phosphorylation of FERM fragments was determined by the ratio of pY397 signals to GST signals.

Molecular dynamics simulations

Explicit solvent MD simulations were performed using Desmond (D.E. Shaw Research; Shivakumar et al., 2010). The OPLS_2005 force field (Jorgensen et al., 1996) was used for protein and the TIP3P model for waters (Jorgensen et al., 1983). Simulations were initiated from the crystal structure of the FAK/FERM domain (Protein Data Bank accession no. 2J0J). Disordered loops were predicted with in-house software (Protein Localization Optimization Program; distributed as Prime by Schrodinger, LLC; Jacobson et al., 2004). The N and C termini were capped to neutralize charges. Ionizable groups were assumed to have model compound-like pK$_a$ values. Histidine side chains were neutralized except for the side chain of interest (i.e., His58). Each model was placed in an orthorhombic water box with a minimum of 10 Å from any protein heavy atom to the edge of the box. Counterions were added to make the system electrically neutral, and NaCl concentration was set at 0.1 M. Trajectories converged to a stable state as measured by backbone RMSD and total energy within the first 3 ns of each simulation. The final 5 ns of each simulation were used for analysis. Trajectories were clustered by single linkage analysis using a cutoff of 0.07 nM. VMD (Humphrey et al., 1996) was used for visualization.

Statistics

Statistical significance (P values) was determined by Student's *t* test (unpaired, two-tailed) using Prism software (GraphPad).

Online supplemental material

Fig. S1 shows NHE1-dependent autophosphorylation of FAK and spreading in various cell lines. Fig. S2 shows calibration of fluorescence ratio of pHluorin and mCherry to pH in both wild-type and NHE1 shRNA MEFs. Fig. S3 shows that activation of integrin with MnCl$_2$ does not restore attenuated FAK pY397 with EIPA. Online supplemental material is available at http://www.jcb. org/cgi/content/full/jcb.201302131/DC1.

References

Almeida, E.A., D. Ilić, Q. Han, C.R. Hauck, F. Jin, H. Kawakatsu, D.D. Schlaepfer, and C.H. Damsky. 2000. Matrix survival signaling: from fibronectin via focal adhesion kinase to c-Jun NH(2)-terminal kinase. *J. Cell Biol.* 149:741–754. http://dx.doi.org/10.1083/jcb.149.3.741

Amith, S.R., and L. Fliegel. 2013. Regulation of the Na+/H+ exchanger (NHE1) in breast cancer metastasis. *Cancer Res.* 73:1259–1264. http://dx.doi.org/10.1158/0008-5472.CAN-12-4031

Arias-Salgado, E.G., S. Lizano, S. Sarkar, J.S. Brugge, M.H. Ginsberg, and S.J. Shattil. 2003. Src kinase activation by direct interaction with the integrin beta cytoplasmic domain. *Proc. Natl. Acad. Sci. USA.* 100:13298–13302. http://dx.doi.org/10.1073/pnas.2336149100

Arold, S.T. 2011. How focal adhesion kinase achieves regulation by linking ligand binding, localization and action. *Curr. Opin. Struct. Biol.* 21:808–813. http://dx.doi.org/10.1016/j.sbi.2011.09.008

Beaumont, K.G., and M. Mrksich. 2012. The mechanostability of isolated focal adhesions is strongly dependent on pH. *Chem. Biol.* 19:711–720. http://dx.doi.org/10.1016/j.chembiol.2012.04.016

Cardone, R.A., V. Casavola, and S.J. Reshkin. 2005. The role of disturbed pH dynamics and the Na+/H+ exchanger in metastasis. *Nat. Rev. Cancer.* 5:786–795. http://dx.doi.org/10.1038/nrc1713

Chacón, M.R., and P. Fazzari. 2011. FAK: dynamic integration of guidance signals at the growth cone. *Cell Adhes. Migr.* 5:52–55. http://dx.doi.org/10.4161/cam.5.1.13681

Cohen, L.A., and J.L. Guan. 2005. Residues within the first subdomain of the FERM-like domain in focal adhesion kinase are important in its regulation. *J. Biol. Chem.* 280:8197–8207. http://dx.doi.org/10.1074/jbc.M412021200

Cooper, L.A., T.L. Shen, and J.L. Guan. 2003. Regulation of focal adhesion kinase by its amino-terminal domain through an autoinhibitory interaction. *Mol. Cell. Biol.* 23:8030–8041. http://dx.doi.org/10.1128/MCB.23.22.8030-8041.2003

Demaurex, N., G.P. Downey, T.K. Waddell, and S. Grinstein. 1996. Intracellular pH regulation during spreading of human neutrophils. *J. Cell Biol.* 133:1391–1402. http://dx.doi.org/10.1083/jcb.133.6.1391

Denker, S.P., and D.L. Barber. 2002. Cell migration requires both ion translocation and cytoskeletal anchoring by the Na-H exchanger NHE1. *J. Cell Biol.* 159:1087–1096. http://dx.doi.org/10.1083/jcb.200208050

Denker, S.P., D.C. Huang, J. Orlowski, H. Furthmayr, and D.L. Barber. 2000. Direct binding of the Na—H exchanger NHE1 to ERM proteins regulates the cortical cytoskeleton and cell shape independently of H(+) translocation. *Mol. Cell.* 6:1425–1436. http://dx.doi.org/10.1016/S1097-2765(00)00139-8

Grinstein, S., M. Woodside, T.K. Waddell, G.P. Downey, J. Orlowski, J. Pouysségur, D.C. Wong, and J.K. Foskett. 1993. Focal localization of the NHE-1 isoform of the Na+/H+ antiport: assessment of effects on intracellular pH. *EMBO J.* 12:5209–5218.

Harguindey, S., S.J. Reshkin, G. Orive, J.L. Arranz, and E. Anitua. 2007. Growth and trophic factors, pH and the Na+/H+ exchanger in Alzheimer's disease, other neurodegenerative diseases and cancer: new therapeutic possibilities and potential dangers. *Curr. Alzheimer Res.* 4:53–65. http://dx.doi.org/10.2174/156720507779939841

Huang, D., M. Khoe, M. Befekadu, S. Chung, Y. Takata, D. Ilic, and M. Bryer-Ash. 2007. Focal adhesion kinase mediates cell survival via NF-kappaB and ERK signaling pathways. *Am. J. Physiol. Cell Physiol.* 292:C1339–C1352. http://dx.doi.org/10.1152/ajpcell.00144.2006

Humphrey, W., A. Dalke, and K. Schulten. 1996. VMD: visual molecular dynamics. *J. Mol. Graph.* 14:33–38: 27–28. http://dx.doi.org/10.1016/0263-7855(96)00018-5

Ilić, D., Y. Furuta, S. Kanazawa, N. Takeda, K. Sobue, N. Nakatsuji, S. Nomura, J. Fujimoto, M. Okada, and T. Yamamoto. 1995. Reduced cell motility and enhanced focal adhesion contact formation in cells from FAK-deficient mice. *Nature.* 377:539–544. http://dx.doi.org/10.1038/377539a0

Ilic, D., B. Kovacic, S. McDonagh, F. Jin, C. Baumbusch, D.G. Gardner, and C.H. Damsky. 2003. Focal adhesion kinase is required for blood vessel morphogenesis. *Circ. Res.* 92:300–307. http://dx.doi.org/10.1161/01.RES.0000055016.36679.23

Ilic, D., M. Mao-Qiang, D. Crumrine, G. Dolganov, N. Larocque, P. Xu, M. Demerjian, B.E. Brown, S.T. Lim, V. Ossovskaya, et al. 2007. Focal adhesion kinase controls pH-dependent epidermal barrier homeostasis by regulating actin-directed Na+/H+ exchanger 1 plasma membrane localization. *Am. J. Pathol.* 170:2055–2067. http://dx.doi.org/10.2353/ajpath.2007.061277

Jacobson, M.P., D.L. Pincus, C.S. Rapp, T.J. Day, B. Honig, D.E. Shaw, and R.A. Friesner. 2004. A hierarchical approach to all-atom protein loop prediction. *Proteins.* 55:351–367. http://dx.doi.org/10.1002/prot.10613

Jorgensen, W.L., J. Chandrasekhar, J.D. Madura, R.W. Impey, and M.L. Klein. 1983. Comparison of simple potential functions for simulating liquid water. *J. Chem. Phys.* 79:926–935. http://dx.doi.org/10.1063/1.445869

Jorgensen, W.L., D.S. Maxwell, and J. Tirado-Rives. 1996. Development and testing of the OPLS all-atom force field on conformational energetics and properties of organic liquids. *J. Am. Chem. Soc.* 118:11225–11236. http://dx.doi.org/10.1021/ja9621760

Karydis, A., M. Jimenez-Vidal, S.P. Denker, and D.L. Barber. 2009. Mislocalized scaffolding by the Na-H exchanger NHE1 dominantly inhibits fibronectin production and TGF-beta activation. *Mol. Biol. Cell.* 20:2327–2336. http://dx.doi.org/10.1091/mbc.E08-08-0842

Koivusalo, M., C. Welch, H. Hayashi, C.C. Scott, M. Kim, T. Alexander, N. Touret, K.M. Hahn, and S. Grinstein. 2010. Amiloride inhibits macropinocytosis by lowering submembranous pH and preventing Rac1 and Cdc42 signaling. *J. Cell Biol.* 188:547–563. http://dx.doi.org/10.1083/jcb.200908086

Kuo, J.C., X. Han, C.T. Hsiao, J.R. Yates III, and C.M. Waterman. 2011. Analysis of the myosin-II-responsive focal adhesion proteome reveals a role for β-Pix in negative regulation of focal adhesion maturation. *Nat. Cell Biol.* 13:383–393. http://dx.doi.org/10.1038/ncb2216

Li, S., S. Sato, X. Yang, P.A. Preisig, and R.J. Alpern. 2004. Pyk2 activation is integral to acid stimulation of sodium/hydrogen exchanger 3. *J. Clin. Invest.* 114:1782–1789.

Lietha, D., X. Cai, D.F. Ceccarelli, Y. Li, M.D. Schaller, and M.J. Eck. 2007. Structural basis for the autoinhibition of focal adhesion kinase. *Cell.* 129:1177–1187. http://dx.doi.org/10.1016/j.cell.2007.05.041

Lim, S.T., D. Mikolon, D.G. Stupack, and D.D. Schlaepfer. 2008. FERM control of FAK function: implications for cancer therapy. *Cell Cycle.* 7:2306–2314.

McLean, G.W., N.H. Komiyama, B. Serrels, H. Asano, L. Reynolds, F. Conti, K. Hodivala-Dilke, D. Metzger, P. Chambon, S.G. Grant, and M.C. Frame. 2004. Specific deletion of focal adhesion kinase suppresses tumor formation and blocks malignant progression. *Genes Dev.* 18:2998–3003. http://dx.doi.org/10.1101/gad.316304

Nikolopoulos, S.N., and F.G. Giancotti. 2005. Netrin-integrin signaling in epithelial morphogenesis, axon guidance and vascular patterning. *Cell Cycle.* 4:e131–e135. http://dx.doi.org/10.4161/cc.4.3.1547

Owen, J.D., P.J. Ruest, D.W. Fry, and S.K. Hanks. 1999. Induced focal adhesion kinase (FAK) expression in FAK-null cells enhances cell spreading and migration requiring both auto- and activation loop phosphorylation sites and inhibits adhesion-dependent tyrosine phosphorylation of Pyk2. *Mol. Cell. Biol.* 19:4806–4818.

Paradise, R.K., D.A. Lauffenburger, and K.J. Van Vliet. 2011. Acidic extracellular pH promotes activation of integrin α(v)β(3). *PLoS ONE.* 6:e15746. http://dx.doi.org/10.1371/journal.pone.0015746

Pouysségur, J., C. Sardet, A. Franchi, G. L'Allemain, and S. Paris. 1984. A specific mutation abolishing Na+/H+ antiport activity in hamster fibroblasts precludes growth at neutral and acidic pH. *Proc. Natl. Acad. Sci. USA.* 81:4833–4837. http://dx.doi.org/10.1073/pnas.81.15.4833

Provenzano, P.P., D.R. Inman, K.W. Eliceiri, H.E. Beggs, and P.J. Keely. 2008. Mammary epithelial-specific disruption of focal adhesion kinase retards tumor formation and metastasis in a transgenic mouse model of human breast cancer. *Am. J. Pathol.* 173:1551–1565. http://dx.doi.org/10.2353/ajpath.2008.080308

Pylayeva, Y., K.M. Gillen, W. Gerald, H.E. Beggs, L.F. Reichardt, and F.G. Giancotti. 2009. Ras- and PI3K-dependent breast tumorigenesis in mice and humans requires focal adhesion kinase signaling. *J. Clin. Invest.* 119:252–266.

Schaller, M.D., C.A. Otey, J.D. Hildebrand, and J.T. Parsons. 1995. Focal adhesion kinase and paxillin bind to peptides mimicking beta integrin cytoplasmic domains. *J. Cell Biol.* 130:1181–1187. http://dx.doi.org/10.1083/jcb.130.5.1181

Schönichen, A., B.A. Webb, M.P. Jacobson, and D.L. Barber. 2013. Considering protonation as a posttranslational modification regulating protein structure and function. *Annu Rev Biophys.* 42:289–314. http://dx.doi.org/10.1146/annurev-biophys-050511-102349

Schwartz, M.A., C. Lechene, and D.E. Ingber. 1991. Insoluble fibronectin activates the Na/H antiporter by clustering and immobilizing integrin alpha 5 beta 1, independent of cell shape. *Proc. Natl. Acad. Sci. USA.* 88:7849–7853. http://dx.doi.org/10.1073/pnas.88.17.7849

Shivakumar, D., J. Williams, Y. Wu, W. Damm, J. Shelley, and W. Sherman. 2010. Prediction of absolute solvation free energies using molecular

dynamics free energy perturbation and the OPLS force field. *J. Chem. Theory Comput.* 6:1509–1519. http://dx.doi.org/10.1021/ct900587b

Sieg, D.J., C.R. Hauck, and D.D. Schlaepfer. 1999. Required role of focal adhesion kinase (FAK) for integrin-stimulated cell migration. *J. Cell Sci.* 112:2677–2691.

Sieg, D.J., C.R. Hauck, D. Ilic, C.K. Klingbeil, E. Schaefer, C.H. Damsky, and D.D. Schlaepfer. 2000. FAK integrates growth-factor and integrin signals to promote cell migration. *Nat. Cell Biol.* 2:249–256. http://dx.doi.org/10.1038/35010517

Srivastava, J., D.L. Barber, and M.P. Jacobson. 2007. Intracellular pH sensors: design principles and functional significance. *Physiology (Bethesda).* 22:30–39. http://dx.doi.org/10.1152/physiol.00035.2006

Srivastava, J., G. Barreiro, S. Groscurth, A.R. Gingras, B.T. Goult, D.R. Critchley, M.J. Kelly, M.P. Jacobson, and D.L. Barber. 2008. Structural model and functional significance of pH-dependent talin-actin binding for focal adhesion remodeling. *Proc. Natl. Acad. Sci. USA.* 105:14436–14441. http://dx.doi.org/10.1073/pnas.0805163105

Stehbens, S., H. Pemble, L. Murrow, and T. Wittmann. 2012. Imaging intracellular protein dynamics by spinning disk confocal microscopy. *Methods Enzymol.* 504:293–313. http://dx.doi.org/10.1016/B978-0-12-391857-4.00015-X

Tavora, B., S. Batista, L.E. Reynolds, S. Jadeja, S. Robinson, V. Kostourou, I. Hart, M. Fruttiger, M. Parsons, and K.M. Hodivala-Dilke. 2010. Endothelial FAK is required for tumour angiogenesis. *EMBO Mol Med.* 2:516–528. http://dx.doi.org/10.1002/emmm.201000106

Tominaga, T., and D.L. Barber. 1998. Na-H exchange acts downstream of RhoA to regulate integrin-induced cell adhesion and spreading. *Mol. Biol. Cell.* 9:2287–2303. http://dx.doi.org/10.1091/mbc.9.8.2287

Webb, B.A., M. Chimenti, M.P. Jacobson, and D.L. Barber. 2011. Dysregulated pH: a perfect storm for cancer progression. *Nat. Rev. Cancer.* 11:671–677. http://dx.doi.org/10.1038/nrc3110

Webb, D.J., K. Donais, L.A. Whitmore, S.M. Thomas, C.E. Turner, J.T. Parsons, and A.F. Horwitz. 2004. FAK-Src signalling through paxillin, ERK and MLCK regulates adhesion disassembly. *Nat. Cell Biol.* 6:154–161. http://dx.doi.org/10.1038/ncb1094